JACS
JOURNAL OF THE AMERICAN CHEMICAL SOCIETY
Article
pubs.acs.org/JACS

Nanoscale Transforming Mineral Phases in Fresh Nacre

Ross T. DeVol,[†] Chang-Yu Sun,[†] Matthew A. Marcus,[‡] Susan N. Coppersmith,[†] Satish C. B. Myneni,[§] and Pupa U.P.A. Gilbert*[,†,∥,⊥,#]

[†]Department of Physics, University of Wisconsin−Madison, 1150 University Avenue, Madison, Wisconsin 53706, United States
[‡]Advanced Light Source, Lawrence Berkeley National Laboratory, 1 Cyclotron Road, Berkeley, California 94720, United States
[§]Department of Geosciences, Princeton University, Princeton, New Jersey 08544, United States
[∥]Department of Chemistry, University of Wisconsin−Madison, 1101 University Avenue, Madison, Wisconsin 53706, United States
[⊥]Radcliffe Institute for Advanced Study, Harvard University, 8 Garden Street, Cambridge, Massachusetts 02138, United States

Supporting Information

ABSTRACT: Nacre, or mother-of-pearl, the iridescent inner layer of many mollusk shells, is a biomineral lamellar composite of aragonite ($CaCO_3$) and organic sheets. Biomineralization frequently occurs via transient amorphous precursor phases, crystallizing into the final stable biomineral. In nacre, despite extensive attempts, amorphous calcium carbonate (ACC) precursors have remained elusive. They were inferred from non-nacre-forming larval shells, or from a residue of amorphous material surrounding mature gastropod nacre tablets, and have only once been observed in bivalve nacre. Here we present the first direct observation of ACC precursors to nacre formation, obtained from the growth front of nacre in gastropod shells from red abalone (*Haliotis rufescens*), using synchrotron spectromicroscopy. Surprisingly, the abalone nacre data show the same ACC phases that are precursors to calcite ($CaCO_3$) formation in sea urchin spicules, and not proto-aragonite or poorly crystalline aragonite (pAra), as expected for aragonitic nacre. In contrast, we find pAra in coral.

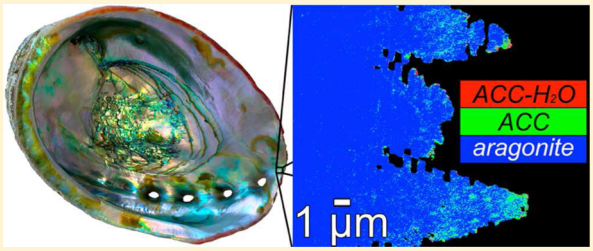

INTRODUCTION

Mollusk shell nacre[1−4] is among the most studied biominerals due to its iridescent lamellar structure,[5,6] its remarkable resistance to fracture,[7−17] and its complex formation mechanisms.[2−4,18−40] An amorphous precursor to nacre formation has been suspected to exist[41,42] but has never been successfully identified, despite extensive attempts. Most fresh nacre studies thus far published focus on the organic matrix,[24,34,43,44] only one of them has focused on the minerals.[45]

In recent years, amorphous calcium carbonate (ACC) minerals have been identified as the first phases deposited by living organisms to form their biominerals, which later become fully crystalline via a series of biologically controlled phase transitions. Sea urchin embryonic spicules were the first biominerals in which an amorphous precursor was discovered,[46] followed by sea urchin spines[47,48] and teeth,[49] bone,[50] tooth enamel,[51] and a variety of other biominerals.[42,52−59] These observations sparked tremendous interest in *in situ* and *in silico* experiments and simulations to understand mineral formation via ACC in abiotic and biological systems.[60−65]

Key *in vitro* experiments are beginning to reveal how the amorphous precursor phases may be stabilized by confinement in pores,[66] between crossed cylinders,[67] in picoliter droplets,[68] within a silica coating,[69,70] and in liposomes,[71−73] all of which prevent release of or contact with water.[68−70,74,75] In sea urchin embryos, such stabilization by confinement takes place in an intracellular vesicle in which ACC is first synthesized and then transported to the biomineralization site.[76,77] Another intriguing possibility is that acidic polymers such as poly-aspartate stabilize ACC in a liquid precursor phase,[78,79] as first demonstrated by the Gower group[80,81] and later re-discovered by molecular dynamics simulations.[63,82]

In vivo, once hydrated amorphous calcium carbonate (ACC-H_2O) is released from the intracellular vesicle, it must be stabilized by other agents, possibly proteins, retarding its dehydration and crystallization. In sea urchin embryonic spicules this function may be carried out by SM50[83] or other proteins.[84] This stabilizing function of proteins, yet to be identified, would prevent the deposited mineral in the forming biomineral from prematurely converting to calcite or aragonite (both naturally occurring crystal forms of calcium carbonate, $CaCO_3$).

The presence of ACC in mature nacre was demonstrated by Nassif et al., who observed by transmission electron microscopy (TEM) that a thin, 2 nm layer of ACC surrounds crystalline aragonite tablets.[42] This is consistent with an ACC precursor to all the aragonite deposited but does not uniquely demonstrate it, because other mechanisms could generate such an ACC lining. For instance, if aragonite crystals grew from solution ion-

Received: July 29, 2015
Published: September 24, 2015

DOI: 10.1021/jacs.5b07931
J. Am. Chem. Soc. 2015, 137, 13325−13333

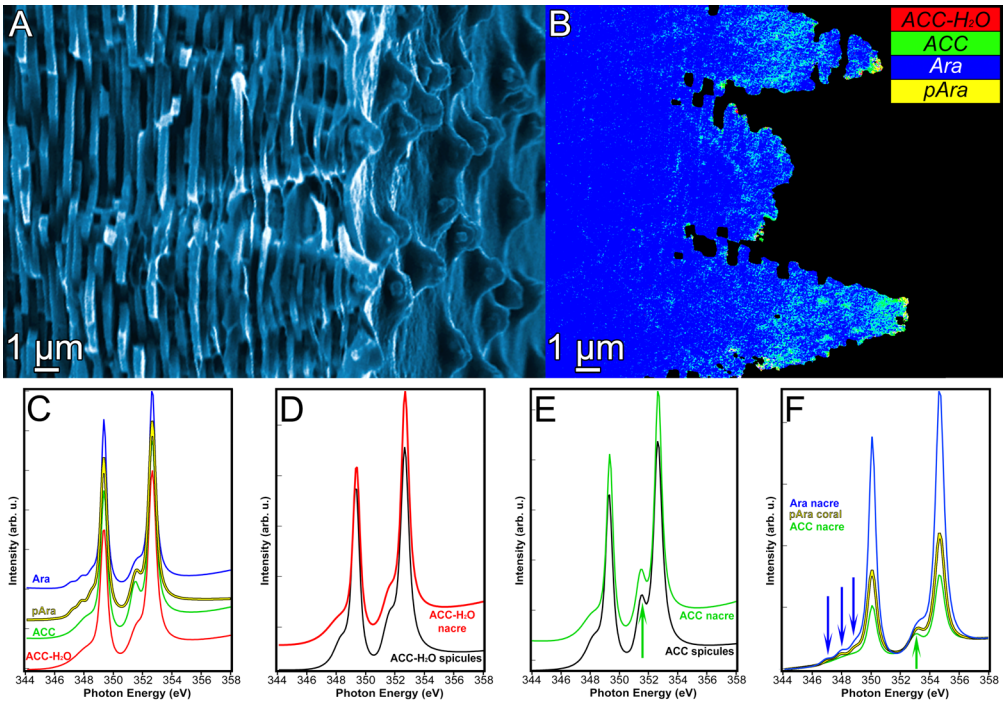

Figure 1. Forming nacre. (A) SEM micrograph of a fractured cross-section of nacre from red abalone, *Haliotis rufescens*. Notice the towers of forming nacre tablets (center), fully formed nacre (left), and the tips of many towers (right). (B) Component map of a nearby fractured cross-section obtained from stacks of PEEM images acquired across the Ca L-edge, after embedding, polishing, and coating. A complete Ca spectrum is acquired at each 20 nm pixel, as described in the Supporting Information, revealing the mineral phases present at that location. In this map, fully formed, space-filling, mature nacre is on the left, three towers of forming nacre tablets are at the center, and Ca-free epoxy appears in black on the right. The results of the component analysis are displayed as a map, in which pixels are assigned different colors depending on the proportions of ACC-H_2O, ACC, proto-aragonite or poorly crystalline aragonite (pAra), and aragonite (Ara) component Ca spectra, as indicated in the color legend. A red, green, blue, or yellow pixel contains only ACC-H_2O, ACC, pAra, or Ara, respectively; pixels containing mixtures are displayed with intermediate color. (C) The four spectral components used for component analysis, color-coded as in the component map in B. Each component spectrum was acquired from single pixels of nacre, as those shown in (B) and as described in the Supporting Information. Comparison of ACC-H_2O (D) and ACC (E) in nacre and in spicules, showing that the spectra are spectroscopically similar in these two biominerals. This is surprising, as sea urchin spicules have calcite as the final phase. (F) Proto-aragonite (pAra) compared to ACC and aragonite (Ara). Notice that the intensity of the two main peaks indicates crystallinity, and is highest in Ara, lowest in ACC, and intermediate in pAra. The line shape of the pAra spectrum has some characteristics of both the other two and is therefore intermediate: the three little peaks (blue arrows, pointing down) that are characteristic of Ara, as well as the calcitic crystal field peak (green arrows, pointing up in E and F). The sea urchin spicule spectra are from ref 83. Spectra in panels C, D, and E are normalized to a pre-edge linear fit of the background and then displaced vertically for clarity. Spectra in panel F are normalized so that the pre- and post-edge intensities are 0 and 1, respectively, so one can compare peak intensities independent of concentration.

by-ion, their growth could be poisoned[85] by organic molecules, resulting in the observed amorphous layer coating each crystal. Zhang and Xu did not observe an amorphous mineral around each tablet in *Perna viridis* mature nacre, but they did in forming nacre tablets.[45] They reported the first evidence of an amorphous mineral in forming nacre tablets, along with disordered nanocrystals, with many different crystal orientations in forming nacre.[45] Addadi et al. showed 50−100 nm nanoparticles after partial etching of nacre tablets and eloquently discussed the possibility that these were originally ACC when first deposited.[41] Dauphin showed with atomic force microscopy that nacre in Nautilus is made of nanoparticles.[86] Oaki and Imai showed particles on the terraced surface of *Pinctada fucata* nacre.[87] Neff showed particles in the cell bodies of mantle cells of *Mercenaria mercenaria*.[88] Those particles were electron-dense, ∼50 nm in size, and did not diffract electrons; it is therefore possible that they were ACC. They could not be nacre precursor particles because *M. mercenaria* is not nacre-forming. The Epple group showed an amorphous material with the short-range order of aragonite in forming snail embryonic shells of *Biomphalaria glabrata*, a gastropod that does not form nacre.[89,90] The mantle cells in general, however, are shell-forming; thus, they also form nacre in nacre-forming species. Jacob et al. recently showed a stable, non-transient ACC phase between the periostracum and the calcite prismatic layer in adult bivalve shells.[91] Again, this must have been deposited by the shell-forming mantle cells. Other authors showed that ACC may contribute to calcite prism formation.[79,92]

These previous lines of evidence make it likely that nacre forms via amorphous precursors, but it has never been directly demonstrated in any gastropod shells. If there are one or more amorphous precursor phases in nacre, they are expected to exhibit the short-range order characteristic of aragonite, according to the polyamorphism idea.[93−101] Polyamorphous precursor phases are structurally distinct, termed proto-calcite, proto-aragonite, and proto-vaterite.[93]

The Epple group observed a biogenic mineral amorphous precursor, with the short-range order of aragonite, in the fresh, forming shell of *B. glabrata*.[89,90] This precursor matures to become either vaterite and aragonite[90] or aragonite only.[89] An aragonite-like form of ACC has been prepared synthetically, in the presence of high Mg:Ca ratios (9:1) or poly-aspartate.[102] Despite its short-range order of aragonite, however, this

DOI: 10.1021/jacs.5b07931
J. Am. Chem. Soc. 2015, 137, 13325−13333

amorphous precursor crystallizes to monohydrocalcite, not aragonite; thus, it does not seem appropriate to call either the biogenic or the synthetic phases proto-aragonite. Proto-vaterite and proto-calcite have been observed and thoroughly investigated,[103] whereas proto-aragonite has been theorized[82,93,98] but not yet experimentally observed.

Here we directly observe the forming part of nacre and analyze its mineral phases with 20 nm resolution, using photoemission electron spectromicroscopy (PEEM) and X-ray absorption near-edge structure (XANES) spectroscopy. For brevity, the combination of these two methods will be hereafter referred to as PEEM.

We recently demonstrated using PEEM that there are not two but three mineral phases in forming sea urchin biominerals:[49,83,104,105] ACC-H_2O, an intermediate phase that is likely anhydrous ACC, and calcite.[105] We observed their distribution in space and time[83] in sea urchin spicules and, using calorimetry, the energetics of their phase transitions.[106]

Whether the same or different transient precursor mineral phases are observed in nacre is a question best addressed using PEEM and freshly sacrificed animals, so the organics and minerals in the shell are as pristine as possible at the time of analysis. After the shells are cut, embedded, polished, and coated as described previously,[107−110] they can be analyzed in cross-section; hence, the nacre layers are seen as separated by parallel lines (organic sheets), and, most importantly, forming and fully formed nacre are analyzed simultaneously, in the same field of view, as presented in Figure 1. Comparing forming and mature nacre is key to interpreting the spectroscopic results and understanding the precursor mineral phases involved in nacre formation. The salient characteristics of a PEEM experiment are that it provides spatial resolution on the order of 20 nm,[4] probes a depth of 3 nm at the Ca L-edge,[108,111] and detects the crystal or amorphous structure in the immediate surrounding of the probed atoms, in this work Ca; therefore, it is most sensitive to the symmetry of atoms bonded to Ca: six and nine oxygen atoms in calcite and aragonite, respectively.

To our knowledge, only one group has reported successful analysis of the mineral phases present in forming nacre using TEM: Zhang and Xu showed non-diffracting material in forming tablets of the bivalve *Perna viridis*, and this appears to be a combination of ACC and nanocrystalline aragonite with disordered orientations.[45]

RESULTS

In Figure 1 we present the characteristic morphology of forming columnar nacre, as observed by scanning electron microscopy (SEM), and its four mineral phases observed by PEEM. Forming nacre exhibits stacks of tablets wider at the base and narrower at the tip, termed "towers".[38] With time each tablet in a tower widens in its nacre layer until it abuts tablets from other towers. They stop growing when the layer between two organic sheets is completely filled with mineral.[31]

As described in the Figure 1 caption, a component map is a spatial distribution of specific reference spectra, termed components. Each component map can be displayed alone as in Figure S1R-Y, or together with other components, as in Figures 1B and S1RGBY. When the components are displayed in RGB or RGBY maps they follow the rules of additive color mixing: yellow = red + green (Y = R + G), magenta = red + blue (M = R + B), and cyan = blue + green (C = B + G).[112]

The most difficult step in this analysis is the production of the best possible reference spectra to be used in component mapping. A detailed description of how such spectra were obtained is provided in the Supporting Information.

In fully formed, mature nacre the phase observed most frequently, almost exclusively, is aragonite, and most of the spectra in forming nacre are also aragonite, as shown by the majority of blue pixels in Figure 1B, and displayed in separate panels in Figure S1. Figure S2 shows the excellent agreement of the aragonite spectra from nacre and geologic aragonite, with only minor differences, possibly due to the <1% anisotropic lattice distortions previously observed in biogenic aragonite from bivalve, gastropod, and cephalopod shells.[113,114] A few pixels in forming nacre, however, are observed to be ACC-H_2O, or proto- or poorly crystalline aragonite (pAra), and many more pixels the same intermediate phase observed in sea urchin spicules and teeth, tentatively interpreted as anhydrous ACC (Figure 1E). All green pixels, and a few red and yellow ones, are phases found mostly in forming nacre, whereas in mature nacre pixels with calcite-like ACC (green pixels) appear sporadically (Figure S1G), and only near the organic sheets, which is consistent with previous TEM observations in mature[42] and forming nacre.[45] The four mineral phases are spectroscopically distinct, and their spectra are presented in Figure 1C.

Unexpectedly, in forming nacre the most abundant non-crystalline phase, ACC, is spectroscopically identical to the same phase observed in sea urchin spicules, as shown in Figure 1E. The intermediate spectra (red and green) are indistinguishable from those in spicules. See comparisons of ACC-H_2O in nacre and sea urchin spicules in Figure 1D and of ACC in nacre and spicules in Figure 1E.

In Ca spectra the line shape represents the symmetry and coordination of Ca atoms, and therefore differs dramatically across calcium carbonate polymorphs.[115] In calcite and aragonite, six and nine oxygen atoms, respectively, coordinate and bond each Ca atom, and seven in ACC.[116] Notice that the peak indicated by the green upward arrow in Figure 1E, which we refer to as peak 2, is prominent in the intermediate "green" phase. This peak is associated with calcite-like six-fold coordination of Ca atoms.[83,105,117] Thus, the data here show that in nacre the precursor ACC phase has calcite-like character even though it is a precursor to aragonite, not calcite formation. This is in contrast with the expected proto-aragonite phase and previous observations in synthetic[94−99] and biogenic[89,90] systems.

The fourth component in Figure 1 could be proto-aragonite or poorly crystalline aragonite (pAra). Ca L-edge spectra from pAra have not been reported previously. We observed these characteristic and unprecedented spectra extensively in coral, another aragonite biomineral, and found this mineral phase concentrated in globular particles at the centers of calcification in *Madracis sp.* coral, as shown in Figure 2. As in nacre in Figure 1, in coral in Figure 2 the most abundant phase is aragonite (blue). Coral, however, has abundant pAra, which nacre lacks almost entirely (Figure S3).

Figure 1C,F shows the pAra reference spectrum, obtained averaging the spectra shown in Figure S4, which are of nearly pure (>80%) pAra, acquired from the centers of calcification in Figure 2 and others. As shown in Figure 1F, the pAra spectrum is intermediate between calcite-like ACC and aragonite: first, it has intermediate crystallinity, as shown by the intensity of the two most intense peaks (L_2 and L_3 edges, termed white lines, or peaks 1 and 3 in this work; see Figures S2 and 3 for peak numbers); second, it has the three little peaks as in aragonite (blue downward arrows in Figure 1, peaks 4′, 4, and 4″ in

DOI: 10.1021/jacs.5b07931
J. Am. Chem. Soc. 2015, 137, 13325−13333

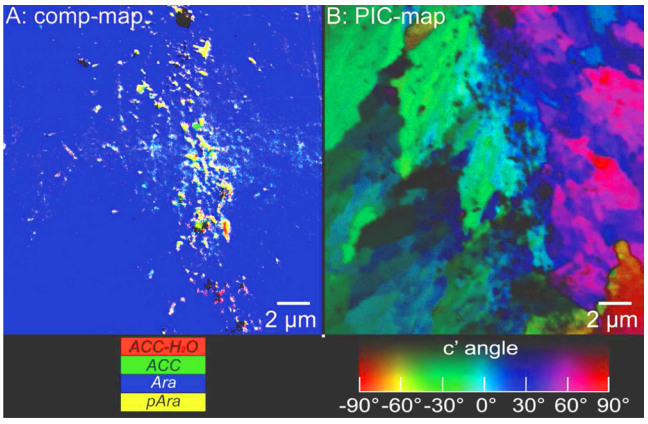

Figure 2. Centers of calcification in a *Madracis sp.* coral polished cross-section. (A) Component map obtained using the same four components and color scheme as in Figure 1, as shown in the color legend. Notice the yellow submicron dots, which are rich in pAra. The full spectra extracted from these and other pAra dots are shown in Figure S4. (B) Polarization-dependent imaging contrast (PIC) map of the same region shown in panel A. Different colors correspond to different orientations of aragonite crystals, according to the color bar at the bottom. Poorly crystalline or amorphous minerals do not exhibit a polarization dependence and therefore appear in black. Notice the submicron black dots scattered vertically at the centers of calcification, which correspond in position to the dots exhibiting pAra spectra in panel A. We therefore conclude that pAra is amorphous.

Figures S2 and 3) and peak 2 at 351.4 eV as in calcite and calcite-like ACC (green upward arrow). It does not, however, have peak 2′ at 351.7 eV, which is characteristic of aragonite. The pAra spectrum has a dip where peak 2′ should be; therefore, this spectrum cannot be a mixture of aragonite and calcite-like ACC. In fact, a linear combination of spectra including any amount of aragonite spectrum would have peak 2′, and thus a total of seven peaks (Figure S2), not six, with two white lines, two crystal field peaks at 351.4 and 351.7 eV, and the three little peaks (green arrows). Spectra from independent acquisitions on coral demonstrate that this is never the case: peak 2′ at 351.7 eV, which is characteristic of crystalline aragonite, is always absent, and peak 2 at 351.4 eV is always well distinct, as shown in Figure S4. However, the three little peaks (blue downward arrows, 4′, 4, and 4″), also characteristic of aragonite and aragonite alone among all calcium carbonates, hydrated and anhydrous,[115] are always present in these unprecedented spectra. We therefore conclude that this phase in coral must be an aragonite-like form of ACC, and thus either proto- or poorly crystalline aragonite, collectively abbreviated pAra for simplicity.

Figure 3 shows peak-fitting of all nacre and coral spectra in Figure 1, plus geologic aragonite and calcite. All fit coefficients are presented in Table S1. Notice that for pAra we used seven Lorentzians, and the one called 2′ at 351.7 eV went to zero amplitude as there really is *not* a peak at that energy, demonstrating that the regions from which this spectrum originated did not contain any fully crystalline aragonite, and that the pAra spectrum cannot be a linear combination of the spectra of ACC and aragonite.

We also note that all spectroscopic data in this work were acquired with circular polarization, thus minimizing the effect of different crystal orientations. The lack of peak 2′ in multiple regions of coral, therefore, cannot be due to the polarization-dependent effect described by Metzler and Rez.[118] Strong evidence for this point is provided by the co-localization in the polarization-dependent imaging contrast (PIC) map of black, non-polarization-dependent, non-crystalline spots in Figure 2A and yellow pAra spots in Figure 2B. Different *b*-axis orientations of aragonite, such as those giving low peak 2′ in ref 118, would still have a strong polarization dependence of the *c*-axis orientation, and would therefore have to be brightly colored in the PIC-map of Figure 2A. Since they are black, we can safely conclude that they are not polarization dependent because they are not crystalline.

In all spectra in Figures 1 and 4, the two main peaks 1 and 3 have greater intensity in aragonite (B) than for any of the amorphous phases (R, G, Y). See Figure 1F for a direct comparison. Sharper, more intense peaks indicate greater crystallinity, as expected.

We now discuss expected and unexpected phase transitions in forming nacre, as detailed in Figure 4. In Figure 4A,B, ACC-H_2O transforms into ACC and then into aragonite by dehydration followed by crystallization, as expected. Figure 4C,D shows a gradual transition from green to blue (G-to-B), which demonstrates a slow crystallization process with coexistence of ACC and aragonite in several pixels (cyan C = G+B). Figure S5 shows key testing done on the spectra of Figure 4 and demonstrates the reliability of component mapping.

An energy landscape for the scenario in Figure 4A–D is presented in Figure 5A, which is based on the enthalpies of transformation measured by Radha et al.,[106] and the activation barriers are qualitatively drawn, as deduced from the data of Figures 1 and 4, and six additional regions from two shells in Figure S6. Because in all these component maps green pixels occur more frequently than red pixels, the energy barrier for the G-to-B transition is greater than that for the R-to-G transition in Figure 4A.

In Figure 4E,F, ACC-H_2O transforms directly into aragonite, almost completely skipping the ACC phase. We therefore see a transition from red to blue with magenta pixels in between (magenta M = R+B), indicating a mixture of the initial and final phases. In Figure 4F, green is 9% in one pixel and 0% in all others. A possible interpretation of this result is that the energy barrier for ACC-H_2O to become ACC (R-to-G) is relatively high, whereas the barrier for ACC to become aragonite (G-to-B) is low, as presented in Figure 5B. In this scenario, ACC-H_2O transformed into ACC slowly, and ACC quickly transformed again into aragonite before it was observed, thus leading to the coexistence of ACC-H_2O and aragonite in the same pixel. It is possible that the green ACC phase is skipped altogether, as contemplated by the Ostwald rule of stages; however, because in some regions we also observe a small but non-zero percentage of green in the magenta pixels (e.g., the 9% above), it is more realistic to hypothesize a low G-to-B activation barrier. This is demonstrated in Figure 4 and Table S2.

The data in Figures 1, 4, and S6 demonstrate that ACC-H_2O and another intermediate phase, previously tentatively assigned to ACC,[49,83,105] are the two amorphous-phase precursors to nacre formation. The observation that these phases are spectroscopically identical to those in sea urchin spicules, where they are precursors to calcite, not aragonite, is unexpected. This observation suggests that the nearest neighboring atoms to Ca have the six-coordinated symmetry of calcite when they are first deposited by the animal (or seven in ACC[116]), but after reaching the biomineralization site they

DOI: 10.1021/jacs.5b07931
J. Am. Chem. Soc. 2015, 137, 13325−13333

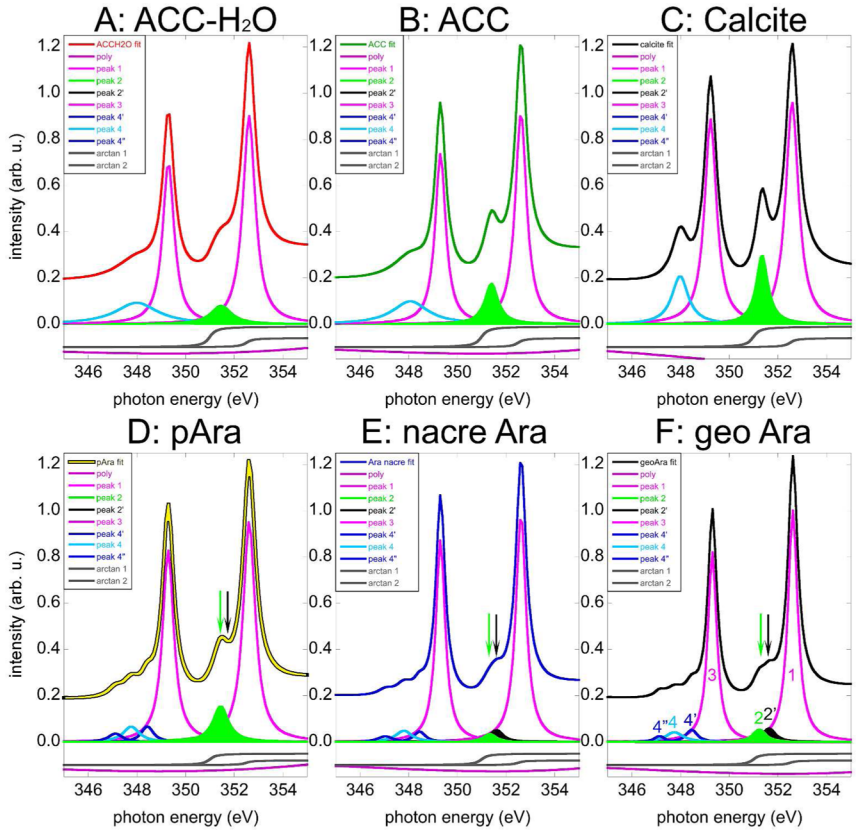

Figure 3. Peak-fitting of the four distinct spectra used for component mapping, as well as geologic aragonite and calcite: (A) ACC-H_2O, (B) ACC, (C) calcite, (D) proto- or poorly crystalline aragonite, (E) aragonite in nacre, and (F) geologic aragonite. All fit coefficients are provided in Table S1, which is color-coded as the individual peaks here. The fit is displaced up and the background polynomial and arctangents down, for clarity. Notice the presence of peak 2 (bright green-shaded peak) in all aragonite and proto-aragonite spectra. Also notice that peak 2′ (black-shaded peak) is present in nacre and geologic aragonite but completely absent from proto-aragonite; in fact, there is a dip in the pAra spectrum at the energy position of peak 2′ (see bright green and black arrows at identical energy positions in panels D, E, and F). Peak-fitting with peak 2′, locking its position and width and setting the amplitude free to change as a fit parameter, yields zero amplitude for this peak in pAra, confirming that peak 2′ does not exist in pAra.

transform to assume the nine-coordinated symmetry of aragonite. Such symmetry transformation must occur rather rapidly, as amorphous phases appear in only a few pixels, with the majority of pixels being blue in Figures 1B and S6. Since we observe more cyan than magenta pixels, we can deduce that the combination of transformation rates in Figure 5A is either slower or more common than that in Figure 5B. In a computer simulation, we produced a three-dimensional model system in which all possible combinations of the two transitions are explored: fast dehydration and slow crystallization, slow and fast, slow and slow, or fast and fast (Figure S7). We observed the greatest agreement with the experimental results in the fast-slow and slow-fast combinations, which are those corresponding to the energy landscapes in Figure 5, panels A and B, respectively. These appear to be localized in different tablets, so they co-exist in nacre in time but not in space, as shown in Figure 4.

The simulation of Figure S7 shows the interplay of these transition rates. Briefly, a three-dimensional cuboid made of voxels transforming from R to G to B is created, and slices are taken to observe transitions. The transformations can be fast or slow, and only occur in a spatially connected fashion. The only simulation results similar to the experimental results in Figures 1, 4, and S6 are obtained for fast and slow or slow and fast transformations (Figure S7A,B, respectively), not for slow and slow or fast and fast (Figure S7C,D, respectively). Specifically, transitions from a red region to a blue region, with an assortment of all other colors at their interfaces, as in Figure S7C,D, are never observed experimentally.

Although it is not possible with the present data to give a quantitative estimate of how fast (or slow) these transitions are, a qualitative idea (Figure 5) clarifies the mechanisms leading to the data of Figures 1, 4, and S6.

In Figure S8, the nanoparticulate texture of cryo-fractured nacre is presented. Although morphology is not a direct indication of formation mechanism, this nanoparticulate morphology, first observed in Nautilus by Dauphin,[86] suggests that nacre formed via attachment of particles.[119−121] From the PEEM results one can infer that these particles were amorphous at the time of attachment and later crystallized to aragonite.

■ DISCUSSION

Lowenstam showed, in a pioneering experiment in 1972, that stable biogenic amorphous calcium phosphate crystallizes to different polymorphs when heated.[100] The same idea, now termed polyamorphism,[93−101] was confirmed by observation of ACC with aragonite-like short-range order in another biomineral, freshwater snail shells, using extended X-ray absorption fine structure (EXAFS) spectroscopy at the calcium

DOI: 10.1021/jacs.5b07931
J. Am. Chem. Soc. 2015, 137, 13325−13333

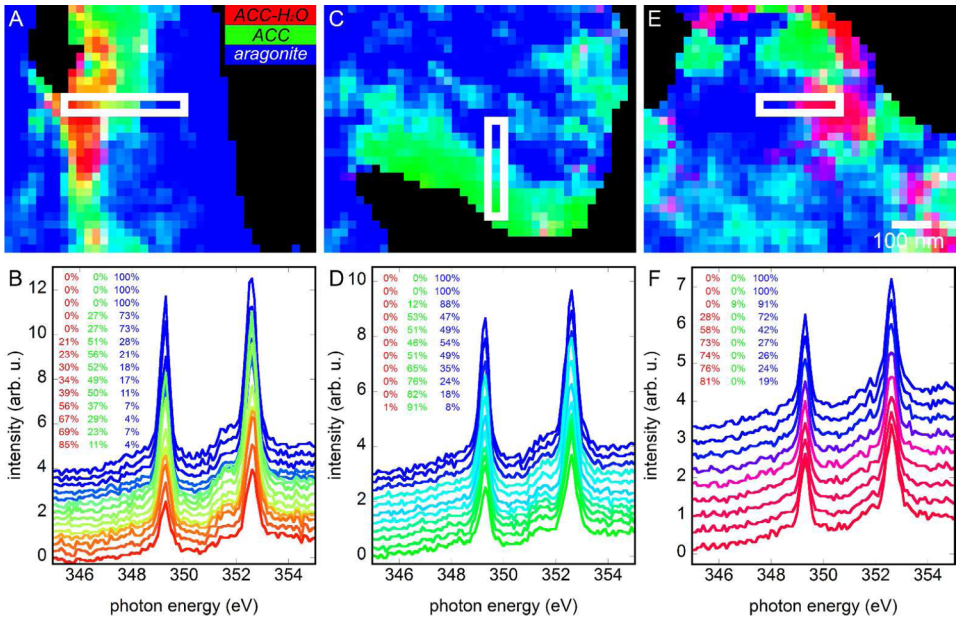

Figure 4. Component maps and spectra of forming nacre. (A,C,E) Zoomed-in component maps showing representative spatial transitions across phases, color-coded as in Figures 1 and 2. The white outlines surround the lines of single 20 nm pixels from which the spectra in panels B, D, and F were extracted. Panels A and B show nacre pixels that transform gradually from pure ACC-H_2O, through intermediate mixture phases shown in orange and yellow, to pure ACC, and finally to aragonite. Panels C and D show a gradual spatial transition from ACC to aragonite, with extensive intermediate mixtures in cyan. Panels E and F show a red-to-blue transition, in which no intermediate green is present, demonstrating that the ACC phase was either present for a very short time or skipped altogether. In panels B, D, and F, the percentages of each component present in each pixel-spectrum are displayed, as obtained from component mapping. These are also presented in Table S2. Figure S5 shows additional evidence for these spectra.

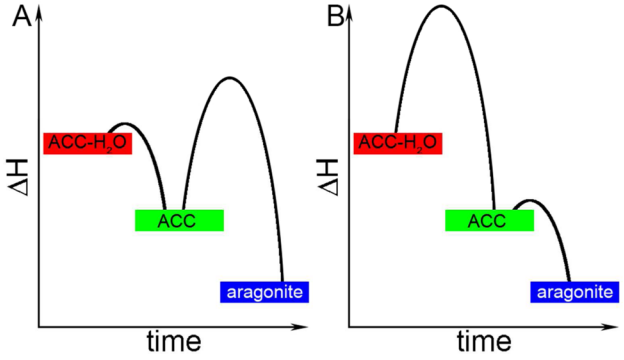

Figure 5. Energy landscapes deduced from nacre component maps and spectra. (A) Energy landscape for R-G-B transitions (e.g., those in Figure 4A,B and 4C,D) and (B) for the R-M-B transition (e.g., that in Figure 4E,F).

K-edge.[89,90] Amorphous mixed with disordered nanocrystalline aragonite was observed by Zhang and Xu in the forming nacre tablets of a green mussel.[45] An aragonite-like precursor phase, therefore, was expected to be observed here in nacre with XANES spectroscopy at the Ca L-edge, as both EXAFS and XANES-PEEM methods are only sensitive to the atomic and electronic structure immediately surrounding Ca atoms. Any aragonite order at any scale would have been detected if it existed in nacre. In this work we show evidence of proto- or poorly crystalline aragonite in coral. We conclude, therefore, that proto- or poorly crystalline aragonite is not a precursor to aragonite in red abalone nacre.

A possibility that cannot be excluded by the present data is that the proto- or poorly crystalline aragonite appears as an intermediate in the crystallization of ACC to aragonite, and it is too short-lived to be detected in the nacre experiments.

Crystallization of ACC particles to aragonite in nacre, however, does not require any pre-existing structural order in the ACC particle itself, because transformation to aragonite may be directed by the pre-existing crystal substrate. Hence, crystal growth, or, more accurately, the propagation of crystallinity at the expense of the amorphous precursors, may be viewed as epitaxial growth.

Epitaxial growth of nacre is consistent with the mineral bridge model first proposed by Schäffer et al.,[27] and then modified and confirmed by Checa et al.[29,38] and Olson et al.[31]

The reproducibility of the data presented here is demonstrated in nine different areas (20 μm × 20 μm each) in two different *Haliotis rufescens* shells, one fixed with ethanol and one with formaldehyde in pH 11 buffer, producing similar and consistent results. In all areas we acquired 2−3 subsequent Ca movies to rule out radiation damage effects, and we observed that exposure to the beam is not likely to have significantly altered the sample at the time of the first movie acquisition. Most frequently we observed identical second movies and slightly damaged third movies. Figure S9 shows zoomed-in regions of repeat movies, demonstrating no significant changes. When/where the changes occur, radiation damage pushes the transitions thermodynamically downhill; hence, it provokes dehydration (R→G) and crystallization to aragonite (G→B). In other words, exposure to X-rays in the PEEM experiment speeds up the same transitions that would occur if the samples were left undisturbed in the animal. The detection of ACC-H_2O and the intermediate phase tentatively assigned to ACC, therefore, cannot be a radiation damage artifact.

DOI: 10.1021/jacs.5b07931
J. Am. Chem. Soc. 2015, 137, 13325−13333

Interestingly, the radiation damage tests are also consistent with epitaxial crystallization to aragonite by direct contact with previously crystalline aragonite, consistent with previous observations of carbonate nucleation and growth *in vitro*.[122−125]

The present 20 nm resolution data, which are also surface sensitive (~3 nm[105,109,111]), succeeded in demonstrating the existence of amorphous precursors to nacre formation. This result has only been published once,[45] despite repeated attempts by many authors. A possible explanation is the extremely limited amount of amorphous phases observed here and their localization to very small regions on the tablet surface. Other spectromicroscopy methods most frequently used in biomineralization experiments, such as infrared and Raman spectroscopies, typically resolve areas on the order of 500 nm or larger, with penetration depths on the order of microns. Limited by such large sampling volumes, forming nacre is spectroscopically identical to mature nacre: the few amorphous voxels are strongly averaged with an overwhelming majority of aragonite voxels. The only other successful observation of amorphous, non-diffracting mineral in nacre was done with high-resolution TEM.[45]

The formation mechanism of nacre is dramatically different from that of sea urchin spicules,[46,83,105,116] spines,[47] and teeth.[49,126] In sea urchins, biomineralization occurs inside a closed membrane that excludes water[76,77] and is in immediate contact with the forming cells. In nacre towers, mineralization occurs extracellularly, near the mantle cells at the tip of the towers, but the base of the towers may be as much as 10 μm away from the nearest cell. ACC crystallizes readily, especially when in contact with water.[106] Therefore, in the space between nacre organic sheets and the growing nacre tablets, there may be sulfate and Mg, shown by Dauphin et al. to persist in bulk nacre,[127−129] to prevent nucleation and crystallization, as well as organic agents that strongly stabilize both ACC-H_2O and ACC phases. The existence of such agents is not only deduced here from geometric considerations, but also demonstrated by the energy diagram in Figure 5 and the data on nacre tablets in Figures 1, 4, and S6, from which this diagram was deduced.

The data presented here show that, unlike coral and freshwater snails, nacre does not form via proto- or poorly crystalline aragonite, but via calcite precursor ACCs, perhaps proto-calcite. This attractive, iconic biomineral provides yet another surprise.

■ ASSOCIATED CONTENT

Supporting Information

The Supporting Information is available free of charge on the ACS Publications website at DOI: 10.1021/jacs.5b07931.

Methods, Figures S1−S9, and Tables S1 and S2 (PDF)

■ AUTHOR INFORMATION

Corresponding Author

*pupa@physics.wisc.edu

Notes

The authors declare no competing financial interest.

[#]Previously publishing as Gelsomina De Stasio.

■ ACKNOWLEDGMENTS

We thank Andreas Scholl, Anthony Young, and Richard Celestre for technical support. P.G. acknowledges support from the National Science Foundation (DMR-1105167), the U.S. Department of Energy (DOE grant DE-FG02-07ER15899), US-Israel Binational Science Foundation (BSF-2010065), and the Radcliffe Institute for Advanced Study at Harvard University. PEEM experiments were done at the Advanced Light Source, supported by DOE grant DE-AC02-05CH11231.

■ REFERENCES

(1) Wise, S. W. *Science* **1970**, *167*, 1486.
(2) Gilbert, P. U. P. A.; Metzler, R. A.; Zhou, D.; Scholl, A.; Doran, A.; Young, A.; Kunz, M.; Tamura, N.; Coppersmith, S. N. *J. Am. Chem. Soc.* **2008**, *130*, 17519.
(3) Metzler, R. A.; Evans, J. S.; Killian, C. E.; Zhou, D.; Churchill, T. H.; Appathurai, N. P.; Coppersmith, S. N.; Gilbert, P. U. P. A. *J. Am. Chem. Soc.* **2010**, *132*, 6329.
(4) Olson, I. C.; Kozdon, R.; Valley, J. W.; Gilbert, P. U. P. A. *J. Am. Chem. Soc.* **2012**, *134*, 7351−7358.
(5) Lowenstam, H. A.; Weiner, S. *On Biomineralization*; Oxford University Press: Oxford, 1989.
(6) Mann, S. *Biomineralization: Principles and Concepts in Bioinorganic Materials Chemistry*; Oxford University Press: New York, 2001.
(7) Barthelat, F.; Espinosa, H. *Exp. Mech.* **2007**, *47*, 311.
(8) Okumura, K.; De Gennes, P.-G. *Eur. Phys. J. E: Soft Matter Biol. Phys.* **2001**, *4*, 121.
(9) Song, F.; Soh, A.; Bai, Y. *Biomaterials* **2003**, *24*, 3623.
(10) Smith, B. L.; Schäffer, T. E.; Viani, M.; Thompson, J. B.; Frederick, N. A.; Kindt, J.; Belcher, A.; Stucky, G. D.; Morse, D. E.; Hansma, P. K. *Nature* **1999**, *399*, 761.
(11) Wang, R.; Wen, H.; Cui, F.; Zhang, H.; Li, H. *J. Mater. Sci.* **1995**, *30*, 2299.
(12) Launey, M. E.; Ritchie, R. O. *Adv. Mater.* **2009**, *21*, 2103.
(13) Li, X.; Xu, Z.-H.; Wang, R. *Nano Lett.* **2006**, *6*, 2301.
(14) Ritchie, R. O. *Nat. Mater.* **2011**, *10*, 817.
(15) Mayer, G. *Science* **2005**, *310*, 1144.
(16) Meyers, M. A.; McKittrick, J.; Chen, P. Y. *Science* **2013**, *339*, 773.
(17) Munch, E.; Launey, M. E.; Alsem, D. H.; Saiz, E.; Tomsia, A. P.; Ritchie, R. O. *Science* **2008**, *322*, 1516.
(18) Wada, K. *Bull. Nat. Pearl Res. Lab.* **1961**, *7*, 703.
(19) Bevelander, G.; Nakahara, H. *Calcif. Tissue Res.* **1969**, *3*, 84.
(20) Mutvei, H. *Scan. Electr. Microsc.* **1979**, *2*, 457.
(21) Lowenstam, H. A. *Science* **1981**, *211*, 1126.
(22) Levi-Kalisman, Y.; Falini, G.; Addadi, L.; Weiner, S. *J. Struct. Biol.* **2001**, *135*, 8.
(23) Currey, J. D. *Science* **2005**, *309*, 253.
(24) Rousseau, M.; Meibom, A.; Gèze, M.; Bourrat, X.; Angellier, M.; Lopez, E. *J. Struct. Biol.* **2009**, *165*, 190.
(25) Addadi, L.; Weiner, S. *Nature* **1997**, *389*, 912.
(26) Belcher, A. M.; Wu, X. H.; Christensen, R. J.; Hansma, P. K.; Stucky, G. D.; Morse, D. E. *Nature* **1996**, *381*, 56.
(27) Schäffer, T. E.; Ionescu-Zanetti, C.; Proksch, R.; Fritz, M.; Walters, D. A.; Almqvist, N.; Zaremba, C. M.; Belcher, A. M.; Smith, B. L.; Stucky, G. D.; et al. *Chem. Mater.* **1997**, *9*, 1731.
(28) Cartwright, J. H.; Checa, A. G. *J. R. Soc., Interface* **2007**, *4*, 491.
(29) Checa, A. G.; Cartwright, J. H.; Willinger, M.-G. *J. Struct. Biol.* **2011**, *176*, 330.
(30) Checa, A. G.; Rodríguez-Navarro, A. B. *Biomaterials* **2005**, *26*, 1071.
(31) Olson, I. C.; Blonsky, A. Z.; Tamura, N.; Kunz, M.; Gilbert, P. U. P. A.; et al. *J. Struct. Biol.* **2013**, *184*, 454.
(32) Olson, I. C.; Gilbert, P. U. P. A. *Faraday Discuss.* **2012**, *159*, 421.
(33) Metzler, R. A.; Abrecht, M.; Olabisi, R. M.; Ariosa, D.; Johnson, C. J.; Frazer, B. H.; Coppersmith, S. N.; Gilbert, P. U. P. A. *Phys. Rev. Lett.* **2007**, *98*, 268102.
(34) Nudelman, F.; Shimoni, E.; Klein, E.; Rousseau, M.; Bourrat, X.; Lopez, E.; Addadi, L.; Weiner, S. *J. Struct. Biol.* **2008**, *162*, 290.
(35) Rousseau, M.; Lopez, E.; Stempflé, P.; Brendlé, M.; Franke, L.; Guette, A.; Naslain, R.; Bourrat, X. *Biomaterials* **2005**, *26*, 6254.

DOI: 10.1021/jacs.5b07931
J. Am. Chem. Soc. 2015, 137, 13325−13333

(36) Nudelman, F.; Gotliv, B. A.; Addadi, L.; Weiner, S. *J. Struct. Biol.* **2006**, *153*, 176.
(37) Cartwright, J. H. E.; Checa, A. G.; Escribano, B.; Sainz-Díaz, C. I. *Proc. Natl. Acad. Sci. U. S. A.* **2009**, *106*, 10499.
(38) Checa, A. G.; Cartwright, J. H. E.; Willinger, M.-G. *Proc. Natl. Acad. Sci. U. S. A.* **2009**, *106*, 38.
(39) Wang, D.; Wallace, A. F.; De Yoreo, J. J.; Dove, P. M. *Proc. Natl. Acad. Sci. U. S. A.* **2009**, *106*, 21511.
(40) Xu, G.; Yao, N.; Aksay, I. A.; Groves, J. T. *J. Am. Chem. Soc.* **1998**, *120*, 11977.
(41) Addadi, L.; Joester, D.; Nudelman, F.; Weiner, S. *Chem. - Eur. J.* **2006**, *12*, 980.
(42) Nassif, N.; Pinna, N.; Gehrke, N.; Antonietti, M.; Jäger, C.; Cölfen, H. *Proc. Natl. Acad. Sci. U. S. A.* **2005**, *102*, 12653.
(43) Kroger, N. *Science* **2009**, *325*, 1351.
(44) Marie, B.; Joubert, C.; Tayalé, A.; Zanella-Cléon, I.; Belliard, C.; Piquemal, D.; Cochennec-Laureau, N.; Marin, F.; Gueguen, Y.; Montagnani, C. *Proc. Natl. Acad. Sci. U. S. A.* **2012**, *109*, 20986.
(45) Zhang, G.; Xu, J. *J. Struct. Biol.* **2013**, *182*, 36.
(46) Beniash, E.; Aizenberg, J.; Addadi, L.; Weiner, S. *Proc. R. Soc. London, Ser. B* **1997**, *264*, 461.
(47) Politi, Y.; Arad, T.; Klein, E.; Weiner, S.; Addadi, L. *Science* **2004**, *306*, 1161.
(48) Seto, J.; Ma, Y.; Davis, S. A.; Meldrum, F.; Gourrier, A.; Kim, Y.-Y.; Schilde, U.; Sztucki, M.; Burghammer, M.; Maltsev, S.; Jäger, C.; Cölfen, H. *Proc. Natl. Acad. Sci. U. S. A.* **2012**, *109*, 3699.
(49) Killian, C. E.; Metzler, R. A.; Gong, Y. T.; Olson, I. C.; Aizenberg, J.; Politi, Y.; Wilt, F. H.; Scholl, A.; Young, A.; Doran, A.; Kunz, M.; Tamura, N.; Coppersmith, S. N.; Gilbert, P. U. P. A. *J. Am. Chem. Soc.* **2009**, *131*, 18404.
(50) Mahamid, J.; Sharir, A.; Addadi, L.; Weiner, S. *Proc. Natl. Acad. Sci. U. S. A.* **2008**, *105*, 12748.
(51) Beniash, E.; Metzler, R. A.; Lam, R. S. K.; Gilbert, P. U. P. A. *J. Struct. Biol.* **2009**, *166*, 133.
(52) Levi-Kalisman, Y.; Raz, S.; Weiner, S.; et al. *J. Chem. Soc., Dalton Trans.* **2000**, 3977.
(53) Raz, S.; Testeniere, O.; Hecker, A.; Weiner, S.; Luquet, G. *Biol. Bull.* **2002**, *203*, 269.
(54) Weiss, I. M.; Tuross, N.; Addadi, L.; Weiner, S. *J. Exp. Zool.* **2002**, *293*, 478.
(55) Dillaman, R.; Hequembourg, S.; Gay, M. *J. Morphol.* **2005**, *263*, 356.
(56) Neues, F.; Ziegler, A.; Epple, M. *CrystEngComm* **2007**, *9*, 1245.
(57) Gago-Duport, I.; Briones, M. J. I.; Rodriguez, J. B.; Covelo, B. *J. Struct. Biol.* **2008**, *162*, 422.
(58) Lee, M. R.; Hodson, M. E.; Langworthy, G. N. *Mineral. Mag.* **2008**, *72*, 257.
(59) Addadi, L.; Raz, S.; Weiner, S. *Adv. Mater.* **2003**, *15*, 959.
(60) Couradeau, E.; Benzerara, K.; Gerard, E.; Moreira, D.; Bernard, S.; Brown, G. E.; Lopez-Garcia, P. *Science* **2012**, *336*, 459.
(61) Nielsen, M. H.; Aloni, S.; De Yoreo, J. J. *Science* **2014**, *345*, 1158.
(62) Pouget, E. M.; Bomans, P. H. H.; Goos, J.; Frederik, P. M.; de With, G.; Sommerdijk, N. *Science* **2009**, *323*, 1455.
(63) Wallace, A. F.; Hedges, L. O.; Fernandez-Martinez, A.; Raiteri, P.; Gale, J. D.; Waychunas, G. A.; Whitelam, S.; Banfield, J. F.; De Yoreo, J. J. *Science* **2013**, *341*, 885.
(64) Weiner, S.; Sagi, I.; Addadi, L. *Science* **2005**, *309*, 1027.
(65) Michel, F. M.; MacDonald, J.; Feng, J.; Phillips, B. L.; Ehm, L.; Tarabrella, C.; Parise, J. B.; Reeder, R. J. *Chem. Mater.* **2008**, *20*, 4720.
(66) Loste, E.; Park, R. J.; Warren, J.; Meldrum, F. C. *Adv. Funct. Mater.* **2004**, *14*, 1211.
(67) Stephens, C. J.; Ladden, S. F.; Meldrum, F. C.; Christenson, H. K. *Adv. Funct. Mater.* **2010**, *20*, 2108.
(68) Stephens, C. J.; Kim, Y.-Y.; Evans, S. D.; Meldrum, F. C.; Christenson, H. K. *J. Am. Chem. Soc.* **2011**, *133*, 5210.
(69) Ihli, J.; Wong, W. C.; Noel, E. H.; Kim, Y.-Y.; Kulak, A. N.; Christenson, H. K.; Duer, M. J.; Meldrum, F. C. *Nat. Commun.* **2014**, *5*, 1.
(70) Kellermeier, M.; Melero-Garcia, E.; Glaab, F.; Klein, R.; Drechsler, M.; Rachel, R.; García-Ruiz, J. M.; Kunz, W. *J. Am. Chem. Soc.* **2010**, *132*, 17859.
(71) Tester, C. C.; Brock, R. E.; Wu, C.-H.; Krejci, M. R.; Weigand, S.; Joester, D. *CrystEngComm* **2011**, *13*, 3975.
(72) Tester, C. C.; Whittaker, M. L.; Joester, D. *Chem. Commun.* **2014**, *50*, 5619.
(73) Tester, C. C.; Wu, C.-H.; Weigand, S.; Joester, D. *Faraday Discuss.* **2012**, *159*, 345.
(74) Nakano, E.; Okazaki, K.; Iwamatsu, T. *Biol. Bull.* **1963**, *125*, 125.
(75) Kniprath, E. *Calcif. Tissue Res.* **1974**, *14*, 211.
(76) Vidavsky, N.; Addadi, S.; Mahamid, J.; Shimoni, E.; Ben-Ezra, D.; Shpigel, M.; Weiner, S.; Addadi, L. *Proc. Natl. Acad. Sci. U. S. A.* **2014**, *111*, 39.
(77) Beniash, E.; Addadi, L.; Weiner, S. *J. Struct. Biol.* **1999**, *125*, 50.
(78) Schenk, A. S.; Zope, H.; Kim, Y.-Y.; Kros, A.; Sommerdijk, N. A.; Meldrum, F. C. *Faraday Discuss.* **2012**, *159*, 327.
(79) Wolf, S. E.; Lieberwirth, I.; Natalio, F.; Bardeau, J.-F.; Delorme, N.; Emmerling, F.; Barrea, R.; Kappl, M.; Marin, F. *Faraday Discuss.* **2012**, *159*, 433.
(80) Gower, L. B.; Odom, D. J. *J. Cryst. Growth* **2000**, *210*, 719.
(81) Olszta, M.; Douglas, E.; Gower, L. *Calcif. Tissue Int.* **2003**, *72*, 583.
(82) Demichelis, R.; Raiteri, P.; Gale, J. D.; Quigley, D.; Gebauer, D. *Nat. Commun.* **2011**, *2*, 590.
(83) Gong, Y. U. T.; Killian, C. E.; Olson, I. C.; Appathurai, N. P.; Amasino, A. L.; Martin, M. C.; Holt, L. J.; Wilt, F. H.; Gilbert, P. U. P. A. *Proc. Natl. Acad. Sci. U. S. A.* **2012**, *109*, 6088.
(84) Benson, N. C.; Benson, S. C.; Wilt, F. *Am. J. Anat.* **1989**, *185*, 177.
(85) Land, T. A.; Martin, T. L.; Potapenko, S.; Palmore, G. T.; De Yoreo, J. J. *Nature* **1999**, *399*, 442.
(86) Dauphin, Y. *Palaeontologische Zeitschrift* **2001**, *75*, 113.
(87) Oaki, Y.; Imai, H. *Angew. Chem., Int. Ed.* **2005**, *44*, 6571.
(88) Neff, J. M. *Tissue Cell* **1972**, *4*, 591.
(89) Marxen, J. C.; Becker, W.; Finke, D.; Hasse, B.; Epple, M. *J. Mollusc Studies* **2003**, *69*, 113.
(90) Hasse, B.; Ehrenberg, H.; Marxen, J. C.; Becker, W.; Epple, M. *Chem. - Eur. J.* **2000**, *6*, 3679.
(91) Jacob, D.; Wirth, R.; Soldati, A.; Wehrmeister, U.; Schreiber, A. *J. Struct. Biol.* **2011**, *173*, 241.
(92) Baronnet, A.; Cuif, J.-P.; Dauphin, Y.; Farre, B.; Nouet, J. *Mineral. Mag.* **2008**, *72*, 617.
(93) Cartwright, J. H.; Checa, A. G.; Gale, J. D.; Gebauer, D.; Sainz-Díaz, C. I. *Angew. Chem., Int. Ed.* **2012**, *51*, 11960.
(94) Chen, S.-F.; Cölfen, H.; Antonietti, M.; Yu, S.-H. *Chem. Commun.* **2013**, *49*, 9564.
(95) Rez, P.; Sinha, S.; Gal, A. *J. Appl. Crystallogr.* **2014**, *47*, 1651.
(96) Constantz, B. R.; Bewernitz, M. A.; Camiré, C. L.; Kang, S.-H.; Schneider, J.; Wade, R. R., II Bioinspired Concrete. In *Biotechnologies and Biomimetics for Civil Engineering*; Pacheco Torgal, F., Labrincha, F., Diamanti, M. V., Yu, C.-P., Lee, H. K., Eds.; Springer: Berlin, 2015; p 297.
(97) Fernandez-Martinez, A.; Kalkan, B.; Clark, S. M.; Waychunas, G. A. *Angew. Chem.* **2013**, *125*, 8512.
(98) Raiteri, P.; Demichelis, R.; Gale, J. D.; Kellermeier, M.; Gebauer, D.; Quigley, D.; Wright, L. B.; Walsh, T. R. *Faraday Discuss.* **2012**, *159*, 61.
(99) Ruiz-Agudo, E.; Cizer, O.; Kudlacz, K.; Rodriguez-Navarro, C. *Abstr. Pap. Am. Chem. Soc.* **2014**, *247*, GEOC-25.
(100) Lowenstam, H. A. *Chem. Geol.* **1972**, *9*, 153.
(101) Saika-Voivod, I.; Poole, P. H.; Sciortino, F. *Nature* **2001**, *412*, 514.
(102) Lam, R. S.; Charnock, J. M.; Lennie, A.; Meldrum, F. C. *CrystEngComm* **2007**, *9*, 1226.
(103) Gebauer, D.; Gunawidjaja, P. N.; Ko, J.; Bacsik, Z.; Aziz, B.; Liu, L.; Hu, Y.; Bergström, L.; Tai, C. W.; Sham, T. K.; et al. *Angew. Chem.* **2010**, *122*, 9073.

DOI: 10.1021/jacs.5b07931
J. Am. Chem. Soc. 2015, 137, 13325−13333

(104) Gilbert, P. U. P. A.; Wilt, F. H. In *Molecular Biomineralization*; Müller, W. E. G., Ed.; Springer: Heidelberg, 2011; p 199.
(105) Politi, Y.; Metzler, R. A.; Abrecht, M.; Gilbert, B.; Wilt, F. H.; Sagi, I.; Addadi, L.; Weiner, S.; Gilbert, P. U. P. A. *Proc. Natl. Acad. Sci. U. S. A.* **2008**, *105*, 17362.
(106) Radha, A. V.; Forbes, T. Z.; Killian, C. E.; Gilbert, P. U. P. A.; Navrotsky, A. *Proc. Natl. Acad. Sci. U. S. A.* **2010**, *107*, 16438.
(107) De Stasio, G.; Frazer, B. H.; Gilbert, B.; Richter, K. L.; Valley, J. W. *Ultramicroscopy* **2003**, *98*, 57.
(108) Frazer, B. H.; Girasole, M.; Wiese, L. M.; Franz, T.; De Stasio, G. *Ultramicroscopy* **2004**, *99*, 87.
(109) Gilbert, P. U. P. A. In *Biomineralization Handbook, Characterization of Biominerals and Biomimetic Materials*; DiMasi, E., Gower, L. B., Eds.; CRC Press: Boca Raton, FL, 2014; p 135.
(110) Gilbert, B.; Andres, R.; Perfetti, P.; Margaritondo, G.; Rempfer, G.; De Stasio, G. *Ultramicroscopy* **2000**, *83*, 129.
(111) Frazer, B. H.; Gilbert, B.; Sonderegger, B. R.; De Stasio, G. *Surf. Sci.* **2003**, *537*, 161.
(112) Gilbert, P. U. P. A.; Haeberli, W. *Physis in the Arts*, rev. ed.; Academic Press-Elsevier: Burlington, MA, 2011.
(113) Pokroy, B.; Quintana, J. P.; Caspi, E. N.; Berner, A.; Zolotoyabko, E. *Nat. Mater.* **2004**, *3*, 900.
(114) Pokroy, B.; Fitch, A. N.; Lee, P. L.; Quintana, J. P.; Caspi, E. N.; Zolotoyabko, E. *J. Struct. Biol.* **2006**, *153*, 145.
(115) DeVol, R. T.; Metzler, R. A.; Kabalah-Amitai, L.; Pokroy, B.; Politi, Y.; Gal, A.; Addadi, L.; Weiner, S.; Fernandez-Martinez, A.; Demichelis, R.; et al. *J. Phys. Chem. B* **2014**, *118*, 8449.
(116) Politi, Y.; Levi-Kalisman, Y.; Raz, S.; Wilt, F.; Addadi, L.; Weiner, S.; Sagi, I. *Adv. Funct. Mater.* **2006**, *16*, 1289.
(117) Rez, P.; Blackwell, A. *J. Phys. Chem. B* **2011**, *115*, 11193.
(118) Metzler, R. A.; Rez, P. *J. Phys. Chem. B* **2014**, *118*, 6758.
(119) De Yoreo, J. J.; Gilbert, P. U. P. A.; Sommerdijk, N. A. M. J.; Penn, R. L.; Whitelam, S.; Joester, D.; Zhang, H. Z.; Rimer, J. D.; Navrotsky, A.; Banfield, J. F.; Wallace, A. F.; Michel, F. M.; Meldrum, F. C.; Cölfen, H.; Dove, P. M. *Science* **2015**, *349*, aaa6760.
(120) Gal, A.; Kahil, K.; Vidavsky, N.; DeVol, R. T.; Gilbert, P. U.; Fratzl, P.; Weiner, S.; Addadi, L. *Adv. Funct. Mater.* **2014**, *24*, 5420.
(121) Gal, A.; Weiner, S.; Addadi, L. *CrystEngComm* **2015**, *17*, 2606.
(122) Elhadj, S.; De Yoreo, J. J.; Hoyer, J. R.; Dove, P. M. *Proc. Natl. Acad. Sci. U. S. A.* **2006**, *103*, 19237.
(123) Giuffre, A. J.; Hamm, L. M.; Han, N.; De Yoreo, J. J.; Dove, P. M. *Proc. Natl. Acad. Sci. U. S. A.* **2013**, *110*, 9261.
(124) Hamm, L. M.; Giuffre, A. J.; Han, N.; Tao, J.; Wang, D.; De Yoreo, J. J.; Dove, P. M. *Proc. Natl. Acad. Sci. U. S. A.* **2014**, *111*, 1304.
(125) Laanait, N.; Callagon, E. B.; Zhang, Z.; Sturchio, N. C.; Lee, S. S.; Fenter, P. *Science* **2015**, *349*, 1330.
(126) Killian, C. E.; Metzler, R. A.; Gong, Y. U. T.; Churchill, T. H.; Olson, I. C.; Trubetskoy, V.; Christensen, M. B.; Fournelle, J. H.; De Carlo, F.; Cohen, S.; Mahamid, J.; Wilt, F. H.; Scholl, A.; Young, A.; Doran, A.; Coppersmith, S. N.; Gilbert, P. U. P. A. *Adv. Funct. Mater.* **2011**, *21*, 682.
(127) Dauphin, Y.; Cuif, J.-P.; Salome, M. *Eur. J. Mineral* **2014**, *26*, 485.
(128) Dauphin, Y.; Cuif, J. P.; Salome, C.; Susini, J. *Am. Mineral.* **2005**, *90*, 1748.
(129) Farre, B.; Brunelle, A.; Laprevote, O.; Cuif, J.-P.; Williams, C. T.; Dauphin, Y. *Comp. Biochem. Physiol., Part B: Biochem. Mol. Biol.* **2011**, *159*, 131.

DOI: 10.1021/jacs.5b07931
J. Am. Chem. Soc. 2015, 137, 13325−13333